In-Situ Chlorine Generation and Rare Earth Chlorination by Molten Salt Electrolysis

Mark Schvaneveldt[1], Tyler Williams[1z], Ranon Fuller[1], Devin Rappleye[1]

[1]Chemical Engineering Department, Brigham Young University, Provo, Utah

[2]Present Address - Argonne National Laboratory, Illinois

[z] Email: wtylerb@byu.edu

ORCID Information

Mark Schvaneveldt – n/a

Tyler Williams - 0000-0002-7206-114X

Ranon Fuller - 0000-0002-5540-0197

Devin Rappleye - 0000-0002-4008-7193

This is an Accepted Manuscript of an article published by Taylor & Francis in *Nuclear Technology* on February 28th 2024, available at: https://doi.org/10.1080/00295450.2023.2299908

Keywords: molten chlorides, actinide-lanthanide separation, electrolysis, chloride volatility

Abstract

Chloride volatility processes for purifying actinide and rare-earth elements have historically required the use of Cl_2 tanks. To minimize the hazards associated with these processes, an apparatus was designed to produce Cl_2 via molten salt electrolysis. Within this apparatus, one can generate Cl_2, chlorinate metals, and consume excess Cl_2. Here, electrode materials were tested for their ability to generate Cl_2, the composition of the gaseous electrolysis product was evaluated using a quadrupole mass spectrometer, and a Ce-foil sample was successfully chlorinated using the electrochemically generated Cl_2.

1. Introduction

Actinide and rare-earth elements (REEs) are critical for current and future technologies. Because of their radioactive properties, actinides are used in spectroscopy, cancer treatment, thermoelectric generators, nuclear energy, and other essential applications. On the other hand, REEs are often used in catalysts, magnets, electronics, ceramics, glasses, and as surrogates for actinides [1]. Both actinides and REEs are strategically important to governments, are found in high level waste forms, and cannot easily be replaced in communication, transportation, and national defense applications [2–4].

Some current processing methods for actinides include solvent extraction, electrorefining, salt distillation, actinide drawdown, and fluoride volatility [5,6]. However, these methods typically produce additional radioactive waste [5,7]. In addition, these processes are limited by surface area constraints (electrorefining), batch processing, and suboptimal yields (actinide

This is an Accepted Manuscript of an article published by Taylor & Francis in *Nuclear Technology* on February 28th 2024, available at: https://doi.org/10.1080/00295450.2023.2299908

drawdown) [8]. Fluoride volatility improves on some of these weaknesses, but fluorination requires highly hazardous chemicals making their use suboptimal [6].

The chloride volatility process has potential to improve actinide and REE refining and has been proposed for pyro-refining [2,5,9,10]. In this process, Cl_2 gas, sometimes with H_2 or CCl_4, reacts with actinides and/or REEs to produce their respective chlorides [2,5,9–11]. Because chlorides are more volatile than their respective metals and differ from each other in volatility by several orders of magnitude, they can be selectively volatilized [5,11–17]. Some actinide and REE chlorides have low vapor pressures (<< 1 Pa up to 1073 K), which allows them to be purified once the chlorinated impurities volatilize with a sweeping inert gas. After purification, chlorides may be reduced if metals or non-chloride products are desired. The chloride volatility process may be a viable processing technique that produces very little radioactive waste because no solvents are used.

Notwithstanding its potential, the chloride volatility process also needs improvement. Previous designs used Cl_2 gas tanks, however Cl_2 is a highly toxic and corrosive compound. Any accidental release during transport, installation, delivery, or processing can result in damaged equipment, major injuries, and/or death. Therefore, this project aims to generate Cl_2 by molten salt electrolysis, use it to chlorinate REEs (as a surrogate for actinides), and consume any excess Cl_2 on-site within a single process vessel (i.e., *in-situ*). Figure 1 shows the proposed *in-situ* process. The proposed process removes hazards associated with transporting and storing large volumes of Cl_2, greatly enhancing the safety and usability of the chloride volatility process.

This is an Accepted Manuscript of an article published by Taylor & Francis in *Nuclear Technology* on February 28th 2024, available at: https://doi.org/10.1080/00295450.2023.2299908

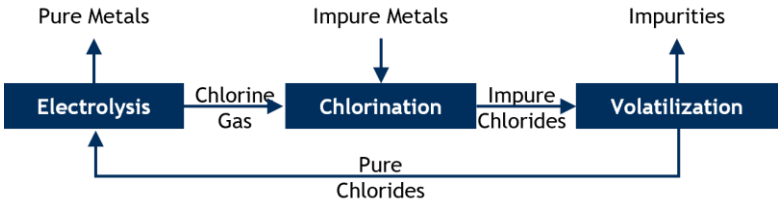

Figure 1. Proposed chloride volatility process.

This process offers an additional safety advantage: in an emergency, the current can be automatically shut off, which immediately stops all production of Cl_2. Molten chloride electrolysis also has the potential ability to simultaneously reduce purified chlorides from the volatilization step (see Figure 1) at the cathode while generating Cl_2 at the anode to chlorinate impure metals (see Figure 2).

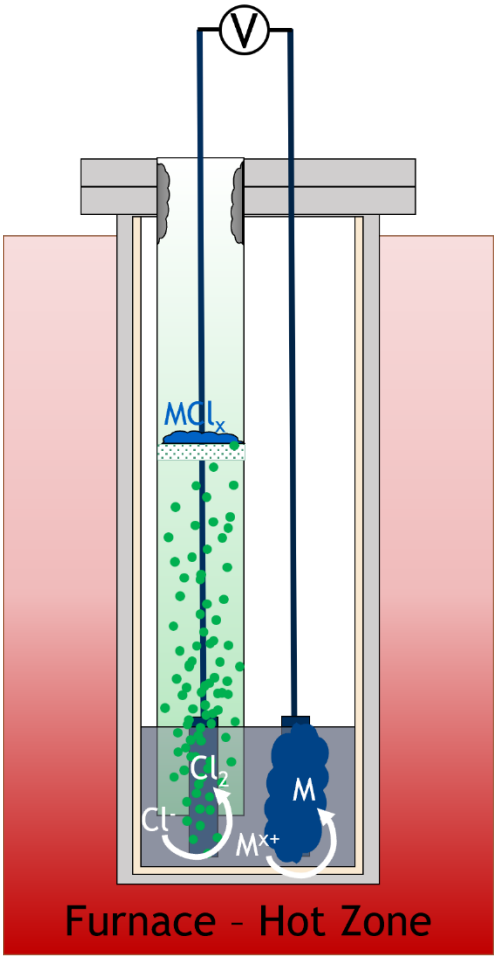

This is an Accepted Manuscript of an article published by Taylor & Francis in *Nuclear Technology* on February 28th 2024, available at: https://doi.org/10.1080/00295450.2023.2299908

Figure 2. Generic schematic for the proposed chloride volatility process.

2. Methods

This work is divided into three sub-categories: (1) electrode performance, (2) Cl_2 generation, and (3) chlorination. Experimental details were described previously [18,19]; the following subsections describe relevant differences. All experiments were conducted in an inert atmosphere glovebox (LC Technologies Inc.) that maintained O_2 and H_2O concentrations below 1 ppm.

Eutectic $LaCl_3$-$CaCl_2$ (28-72 mol%) was melted inside crucibles held in a vertically oriented tube furnace (MTI Corp., OTF-1200X-S-NT). A working electrode (WE), reference electrode (RE), and counter electrode (CE) were inserted in the $LaCl_3$-$CaCl_2$ melt to test electrode materials and generate Cl_2. These electrodes were controlled by an Autolab potentiostat (PGSTAT302N) and their data was analyzed using Autolab's NOVA 2.1 software.

Crucibles of various sizes and materials were used: short alumina crucibles (AdValue Technology, 40 mm OD, 95 mm long) were used for electrode performance tests; taller crucibles, that also acted as a liner for the reactor, were used when substantial amounts of Cl_2 were present. Alumina crucibles (AdValue Technology, >99.6%, 40 mm OD, 95 mm long) were used in Cl_2 generation experiments, while quartz crucibles (University of Utah Glassblowing Facilities, 40 mm OD, 95 mm long) were used for chlorination experiments.

REs were used in all electrochemical tests. These were constructed using closed-ended alumina tubes (AdValue Technology, 6.35 mm OD, 305 mm long) filled with a salt mixture matching the composition of the salt in the crucible as well as approximately 5 mol% AgCl (Alfa

This is an Accepted Manuscript of an article published by Taylor & Francis in *Nuclear Technology* on February 28th 2024, available at: https://doi.org/10.1080/00295450.2023.2299908

Aesar, 99.997%). A silver wire (Alfa Aesar, annealed wire, 99.9%) was then inserted into the tube so that it was in contact with the melted 5 mol% AgCl molten mixture.

2.1 Electrode Performance. A WE material was considered suitable if it could oxidize Cl^- to Cl_2 without being significantly oxidized itself. Tested materials included W (1.5 mm rod, Alfa Aesar, 99.95%), graphite (3.05 mm rod, Alfa Aesar, 99.9995%), Pt-coated Mo (0.457 mm wire, Alfa Aesar, 99.99% Pt, 2 μm thick), Pt (0.25 mm wire, Alfa Aesar, 99.9%), Mo (1 mm wire, Alfa Aesar, 99.94%), and pre-oxidized Ni (1 mm wire, Alfa Aesar, 99.98%). The Ni wire was oxidized by holding it at 1173 K for 2 hours in air [20]. The CE was W (3.175 mm rod, Alfa Aesar, 99.95%). WE geometry was not considered.

2.2 Cl_2 Generation. For Cl_2 generation and chlorination experiments, the WE was a 3.05 mm graphite rod (Alfa Aesar, 99.9995%), dried prior to experimentation in the same manner as the alumina. The CE was a coiled 0.457 mm Pt-coated Mo wire or a coiled 1 mm Mo wire.

Because Cl_2 is corrosive and toxic, several gas-tight apparatuses were constructed to contain it until it could be neutralized. These apparatuses include: (1) a high-temperature reactor, (2) gas and electrode feedthroughs into the reactor, (3) a cold trap, (4) a flow loop outside of the glovebox for mass spectrometry (QMS), and (5) a scrubber to neutralize the Cl_2. A simple process flow diagram (PFD) for the system can be found in Figure 3.

This is an Accepted Manuscript of an article published by Taylor & Francis in *Nuclear Technology* on February 28th 2024, available at: https://doi.org/10.1080/00295450.2023.2299908

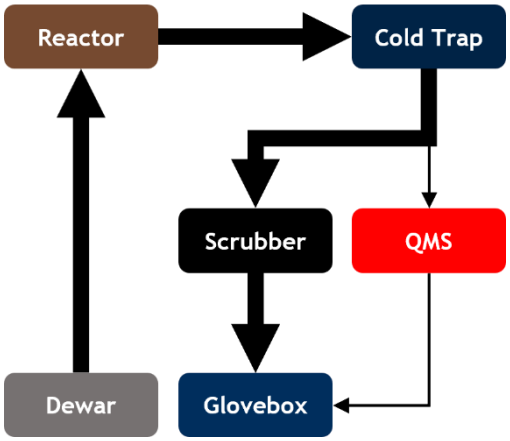

Figure 3. Simplified PFD for gas lines associated with Cl_2 synthesis and analysis. Line thickness indicates relative volumetric flow rates.

2.2.1 High-Temperature Reactor. The reactor (see Figure 4) was made of alloy 200 because Ni resists Cl_2 corrosion at elevated temperatures [21,22]. The bottom half of the reactor was constructed from a schedule 10, 1.5-inch pipe (Continental Steel, alloy 200, 4.27 cm ID, 30.48 cm long) welded to an endplate (Continental Steel, alloy 200) and an open flange (Extreme Bolt, alloy 200). The top half of the reactor was a blind flange (Extreme Bolt, alloy 200) with three threaded holes that were machined to mate with the gas and electrode feedthroughs. The two halves of the reactor were bolted together and sealed with a graphite gasket (McMaster-Carr, high-temperature graphite ring gasket).

This is an Accepted Manuscript of an article published by Taylor & Francis in *Nuclear Technology* on February 28th 2024, available at: https://doi.org/10.1080/00295450.2023.2299908

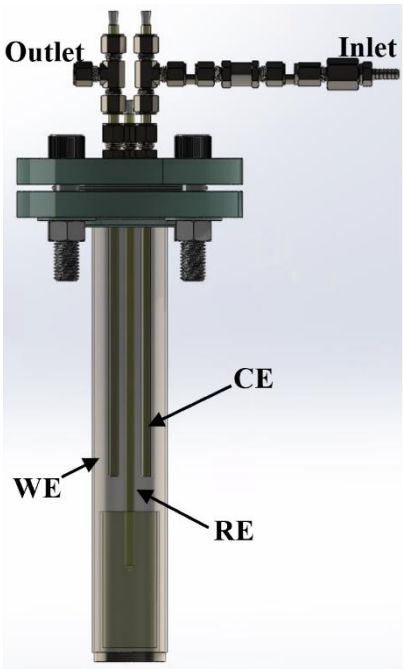

Figure 4. Schematic of reactor featuring interior. Electrodes are missing, but their alumina feedthroughs are present.

2.2.2 Gas and Electrode Feedthroughs. Three feedthroughs provided access into the reactor: one for the RE, one for the CE and gas inlet, and one for the WE and gas outlet. The RE feedthrough was constructed from a straight NPT-to-tube compression fitting. The CE and WE feedthroughs were constructed from (1) a straight NPT-to-tube compression fitting, (2) an alumina tube (AdValue Technology, >99.6%, 6.35 mm), (3) a compression fitting tee, and (4) tapered EPDM plugs through which the electrodes passed.

The RE feedthrough was made gas-tight by tightening an alloy C276 nut over a Teflon ferrule (slid over the outside of the RE's 6.35 mm alumina closed-ended tube) onto the female threads of the tube side for a 0.25-inch (6.35 mm) NPT-to-tube compression fitting (McMaster-Carr, alloy C276, 6.35 mm tube). The NPT threads of this fitting were wrapped in Teflon tape and fastened into the threaded holes in the blind flange.

This is an Accepted Manuscript of an article published by Taylor & Francis in *Nuclear Technology* on February 28th 2024, available at: https://doi.org/10.1080/00295450.2023.2299908

The CE and WE feedthroughs were made gas-tight by: (1) tightening an alloy C276 nut over a Teflon ferrule (slid over the outside of a 6.35 mm alumina tube which electrically insulated the electrode from the reactor) onto the female threads of the tube side for the 0.25-inch NPT-to-tube compression fitting, (2) tightening an alloy C276 nut over another Teflon ferrule (on the same alumina tube) into the female threads for a branch on a compression tee (McMaster-Carr, alloy C276, 6.35 mm tube), (3) tightening an alloy C276 nut over a tapered EPDM plug (through which the WE or CE passed) into the female threads of the other branch on the compression tee, and (4) tightening an alloy C276 nut over the C276 front and back sleeves (slid over the gas inlet or outlet tube) into the stem of the tee. If a fitting leaked, Viton O-rings were added to the ferrules and the seals were further improved by wrapping Teflon tape around the ceramic tubes and stretching the O-rings over the tape.

N_2 (Airgas, UHP200C) or Ar (Airgas, 99.997%) purge gas typically flowed through the reactor while Cl_2 was electrolytically produced to dilute and carry it through the process. The Ar was passed through a purifier (PUR-Gas, MCTG-0080-XX) prior to its introduction into the reactor, which reduced O_2 and H_2O to < 1 ppm. The flow rate of the purge gas was controlled by one of two rotameters for flowrates up to 0.05 LPM or 20 LPM, respectively (Brooks Instrument, Sho-Rate Series).

2.2.3 Cold Trap. The gas exited the reactor via 6.35 mm Teflon tubing and passed through a cold trap to remove species with high vapor pressures (i.e., metal chlorides) at the operating temperature which could clog the lines or deposit inside and damage the QMS. The cold trap consisted of two concentric Teflon tubes (6.35 mm and 12.7 mm), the larger of which was capped. The 6.35 mm tube from the reactor was introduced into the cold trap by a 6.35 mm to 12.7 mm adapter (McMaster-Carr, stainless steel) that was connected to a branch on a 12.7

This is an Accepted Manuscript of an article published by Taylor & Francis in *Nuclear Technology* on February 28th 2024, available at: https://doi.org/10.1080/00295450.2023.2299908

mm tube compression tee (McMaster-Carr, stainless steel). The 6.35 mm tube passed clean through the larger compression tee and out the other branch where it ran for an additional 30 cm. The gas inside the 6.35 mm tube then turned back when it hit the 12.7 mm tube's cap and flowed backwards through the 12.7 mm tube for 30 cm until it reached the 12.7 mm tee and flowed out the stem.

2.2.4 Flow Loop for QMS. Following the cold trap, the cooled gas was sent by a three-way valve with compression fittings (McMaster-Carr, stainless steel) to either the QMS flow loop or directly to the scrubber. If sent to the flow loop, the gas would flow briefly out of the glovebox in a loop made from two 6.35 mm Teflon tubes. At the far end of the flow loop, the two tubes connected into the branches of a compression tee (McMaster-Carr, alloy C276). The capillary inlet for the QMS (Pfeiffer Vacuum, OmniStar GSD 350 O2C 1-200 u, PT-Q81-617-120) sampled the gas at this tee through its stem. This tee was made gas-tight by inserting the capillary through a graphitized Vespel ferrule (Thomas Scientific, 15%/85% graphite/vespel, 1.5875 ID, 6.35 mm OD) held in the compression tee's stem. A Cosmos PS-7 gas detector verified that there were no leaks by sampling the space right next to this compression tee. The QMS's capillary sampled very small volumes of gas (i.e., 1-2 sccm) from the flow loop, recorded the mass spectrometry response, and returned the sampled gas into the glovebox. Unsampled gas continued in the flow loop which terminated at the scrubber.

2.2.5 Scrubber. The scrubber was made of a capped, 2-inch pipe (McMaster-Carr, stainless steel, 15.2 cm long) which was filled with ~150 g Chlorosorb packing (Purafil, 35-45%/15-25%/15-25% carbon/aluminum oxide/carbonic acid-dipotassium salt). After the gas was scrubbed, it was released into the glovebox. Cosmos PS-7 gas detectors monitored Cl_2 and HCl concentrations in the glovebox to validate the scrubber's effectiveness and detect leaks. All

This is an Accepted Manuscript of an article published by Taylor & Francis in *Nuclear Technology* on February 28th 2024, available at: https://doi.org/10.1080/00295450.2023.2299908

Cosmos PS-7 detectors were connected to relays that cut electrolysis power and sounded alarms if gas concentrations reached unsafe levels.

The QMS was calibrated for quantitative concentration measurements using 2000 ppm Cl_2 calibration gas (Calgas, balance N_2). This calibration was deemed sufficient by the QMS's manufacturer for concentration measurements within an order of magnitude. Therefore, Cl_2 generated via electrolysis was diluted with N_2 purge gas to the order of 1000 ppm before quantification with the QMS.

2.3 Chlorination.

Chlorination experiments substituted alumina crucibles with large, custom quartz crucibles. A quartz basket (33 mm OD, 30 mm ID, 50 mm long) was nested in the top of the crucible (see Figure 5). The top of the quartz basket was flared (39 mm OD at the top) to rest on top of the crucible. The base of the basket was a fritted disc (150 μm pores) with three equidistant holes (7 mm OD) to match the gas and electrode feedthroughs. Pores in the fritted discs allowed synthesized Cl_2 to chlorinate the REEs resting on the disc. The larger, equidistant holes allowed electrodes in alumina sheaths to be inserted through the basket and into the molten salt. The same electrodes were used as in the Cl_2 generation tests (see Section 2.2). A second, identical fritted disc (~15 mm above the base) was included to help block volatile chlorides from contaminating the REEs.

This is an Accepted Manuscript of an article published by Taylor & Francis in *Nuclear Technology* on February 28th 2024, available at: https://doi.org/10.1080/00295450.2023.2299908

Figure 5. Quartz Crucible and Basket. Side-by-side (left) and nested (right) views.

When chlorinating, a constant current was applied to the molten salt for 50 minutes. After Cl_2 evolved at the anode, it was convected up to a polished cerium foil (Alfa Aesar, 99.9%, 1 mm thick, 1.25 x 1.25 cm piece) (see Figure 6). After the experiment, Ar (Airgas, 99.997%) pushed excess Cl_2 out of the reactor and cold trap directly into the scrubber, bypassing the QMS. Once the reactor cooled, the remaining cerium foil and metal chlorides were removed. Samples were then taken from the chlorinated metal and analyzed with a Cl^- ion-selective electrode (Vernier, GDX-CL, 10% accuracy, ± 1000 mV range).

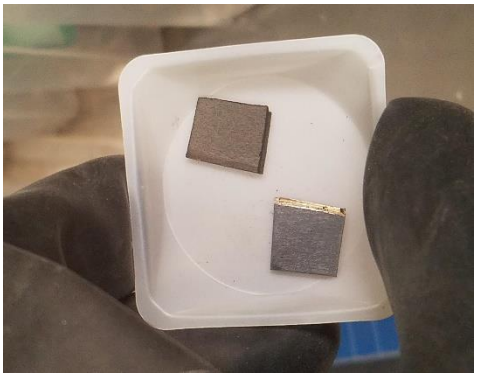

Figure 6. Cerium foil before chlorination. Dark, grey oxide layer removed before chlorination with 220 grit sandpaper.

This is an Accepted Manuscript of an article published by Taylor & Francis in *Nuclear Technology* on February 28th 2024, available at: https://doi.org/10.1080/00295450.2023.2299908

3. Results and Discussion

3.1 Electrode Performance. Cyclic voltammetry was used to evaluate each electrode material's ability to generate Cl_2 without being oxidized itself. Theoretical standard reduction potentials (E^0) for relevant redox couples were calculated relative to the Cl^-/Cl_2 redox pair using a method published by Zhang et al. [23] and data from Barin [24] and NIST JANAF [25]. The results were adjusted to the Ag/AgCl (5 mol%) couple at 1078 K by using the Nernst equation (see Table 1). These calculations do not account for activity effects nor phase changes and only serve as estimations to guide the interpretation of cyclic voltammograms.

Table 1. Estimations of E^0 from thermochemical data.

Redox Couple	***E*⁰ (V vs. Cl^-/Cl_2, 1 atm)**	***E*⁰ (V vs. Ag/AgCl, 5 mol%)**
Ag/Ag^+	-0.814	0.278
Ni/Ni^{2+}	-0.754	0.338
W/W^{2+}	-0.699	0.393
Mo/Mo^{4+}	-0.641	0.451
W/W^{6+}	-0.277	0.815
Mo/Mo^{6+}	-0.140	0.952
Pt/Pt^{2+}	-0.111*	0.981
Cl^-/Cl_2	0.000	1.092
C/C^{4+}	0.215	1.307
*Extrapolated from available thermodynamic data		

Experimental data from cyclic voltammetry can be seen in Figure 7. Although this data cannot give quantitative E^0 data, its results corroborate the general trends seen in Table 1. Mo and W were eliminated because oxidizing currents were observed at potentials more negative than Cl_2 evolution. Pt-coated Mo wire continued approaching the behavior of the Mo wire with each subsequent scan, indicating that its thin Pt layer was not resilient. Both graphite and platinum produced oxidizing currents near the estimated E^0 for Cl_2 generation. Therefore, Pt and graphite were the most suitable of the evaluated electrode materials for Cl_2 generation in molten

This is an Accepted Manuscript of an article published by Taylor & Francis in *Nuclear Technology* on February 28th 2024, available at: https://doi.org/10.1080/00295450.2023.2299908

salts at elevated temperatures. Ultimately, graphite was selected as the candidate electrode material for Cl_2 generation in molten $LaCl_3$-$CaCl_2$ because it resists chlorination at very high temperatures (>700 °C) and is less expensive than Pt.

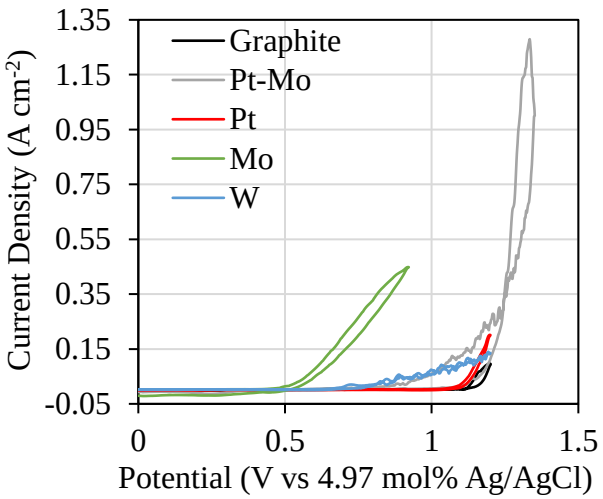

Figure 7. Current density versus potential for 2 wt% $LaCl_3$ in $CaCl_2$ at 825°C and 10 mV s^{-1}, *iR* compensated. 3.174 mm W rod CE.

3.2 Chlorine Generation. The QMS was used to quantify the purity [5] and efficiency of Cl_2 production. 1.5 A was applied to the cell, resulting in a potential of approximately 2 V vs Ag/AgCl (5.24 mol%). Seconds later, the QMS indicated that the relative abundance of Cl_2 increased for ~400 s until it reached a steady-state concentration of ~2600 ppm (see Figure 8) as the generated Cl_2 mixed with N_2 purge gas flowing at 4.1 ± 0.4 LPM. The Cl_2 concentration dropped one minute after electrolysis ended because purge gas was sent through the reactor.

This is an Accepted Manuscript of an article published by Taylor & Francis in *Nuclear Technology* on February 28th 2024, available at: https://doi.org/10.1080/00295450.2023.2299908

Figure 8. Electrochemical (top) and QMS (bottom) response to a current of 1.5 A applied to a Mo/Pt/La/La^{3+},Ca^{2+},Cl^-/Cl_2/$C_{graphite}$ cell (WE geometric area: 2.3 cm^2). Approximately 4 LPM N_2 flowed through the reactor as carrier gas.

The efficiency of Cl_2 production was defined as $x_{Cl2,actual} / x_{Cl2,theoretical}$, where x_{Cl2} is the concentration of Cl_2 (ppm). The value of $x_{Cl2,actual}$ was established using the QMS's calibration and $x_{Cl2,theoretical}$ was determined with

$$\dot{n} = \frac{i}{nF} \tag{1}$$

$$\hat{V} = \frac{RT}{P} \tag{2}$$

$$x_{Cl2,theoretical} = 10^6 \left(\frac{\dot{n}}{\dot{n} + \frac{\dot{V}}{\hat{V}}} \right) \tag{3}$$

where i is current, n is the stoichiometric number of exchanged electrons, F is Faraday's constant, $\dot{n}$ is the theoretical molar flow rate of Cl_2, R is the universal gas constant, T is temperature (298 K), P is pressure (1 bar), $\hat{V}$ is the molar volume of the inert gas, and $\dot{V}$ is the inert gas's flowrate. The efficiency of Cl_2 generation was calculated to be 96.5%, but this is likely underestimated because P was somewhat larger than 1 bar. Other sources of error include the inherent inaccuracies in the rotameter, non-faradaic processes, Cl_2 solubility in the salt, the electrochemical formation of other products besides Cl_2 (i.e., CO and CO_2), and the chlorination of components during the Cl_2's journey to the QMS's detector.

In another experiment, the QMS was used to identify these other products. A current of 1.5 A was applied to the cell, resulting in a potential response greater than 2 V that gradually decreased with several large fluctuations (see Figure 9). These fluctuations may have been due to

This is an Accepted Manuscript of an article published by Taylor & Francis in *Nuclear Technology* on February 28th 2024, available at: https://doi.org/10.1080/00295450.2023.2299908

corrosion of the electrode, changes in the gas-salt-electrode interface, changes in the molten salt composition over time, or a sudden increase of previously exhausted reactants (i.e., O^{2-}) due to bubbles stirring the solution.

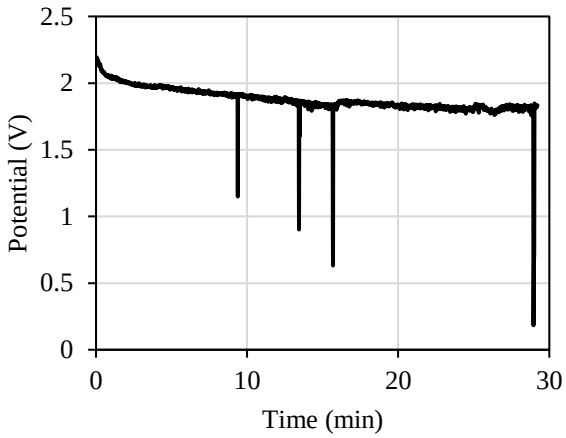

Figure 9. Electrochemical response to a current of 1.5 A applied to a $Mo/Pt/La/La^{3+},Ca^{2+},Cl^{-}/Cl_2/C_{graphite}$ cell (WE geometric area: 2.3 cm^2). Approximately 0.1 LPM of Ar flowed through the reactor as carrier gas.

During electrolysis, the QMS detected increasing signals for mass fragments characteristic of CO, CO_2, HCl, and Cl_2 (i.e., m/z = 28, 44, 36, 70) (see Figure 10). The measured spectra was compared to pure mass spectra (by electron ionization) published by NIST [26] to identify these species. Characteristic fragments for $COCl_2$ and CCl_4 were not found with significant relative abundances, where relative abundance is a normalized measure of the count frequency for a particular m/z ratio, scaled to the magnitude belonging to the most commonly counted m/z ratio. Therefore, a m/z ratio with 3% relative abundance is counted three times per 100 counts of the most common m/z ratio.

This is an Accepted Manuscript of an article published by Taylor & Francis in *Nuclear Technology* on February 28th 2024, available at: https://doi.org/10.1080/00295450.2023.2299908

CO and CO_2 are likely products of the electrochemical reaction between O^{2-} and the graphite anode, where O^{2-} is a hydrolysis product from H_2O in the $CaCl_2$. These hydrolysis [27–33] and electrochemical [34,35] reactions have been investigated elsewhere.

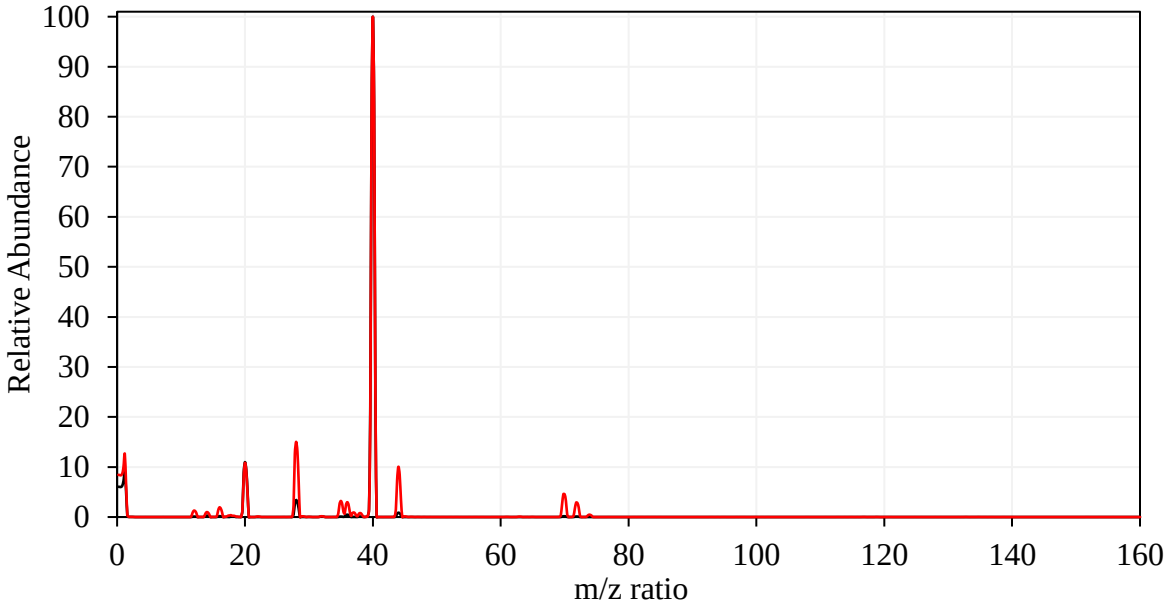

Figure 10. Mass spectra from 30 minutes (black) and 40 minutes (red) into 1.5 A (2.3 cm^2) electrolysis with 0.1 LPM Ar of carrier gas.

3.3 Chlorination. During this experiment, Cl_2 produced by electrolysis convected upward to react with Ce foil resting in the chlorination basket (see Figure 5). The current was set at 1.5 A resulting in a potential greater than 2.5 V with large oscillations (see Figure 11). These oscillations were more frequent than in previous experiments and after 50 minutes, the potential dropped permanently.

This is an Accepted Manuscript of an article published by Taylor & Francis in *Nuclear Technology* on February 28th 2024, available at: https://doi.org/10.1080/00295450.2023.2299908

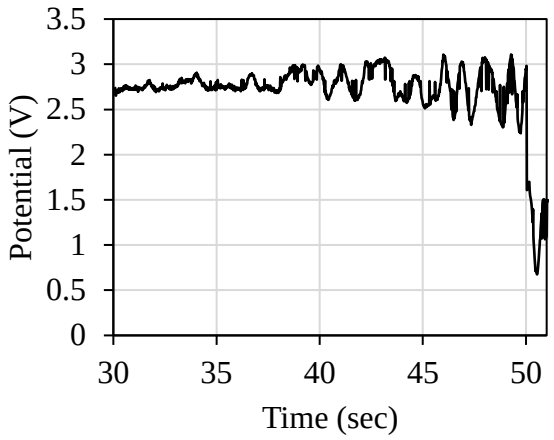

Figure 11. Electrochemical response of 1.5 A applied to a Mo/Pt/La/La^{3+},Ca^{2+},Cl^- /Cl_2/$C_{graphite}$ cell (WE geometric area: 1.77 cm^2). No Ar was pushed through the reactor during electrolysis.

After chlorination, the Ce foil's surface was covered in gray powder, characteristic of $CeCl_3$ (see Figure 12). Of the 52 mg of powder recovered, 97 ± 10% was confirmed to be chloride with a Cl^- ion-selective electrode. Rough calculations indicated that only 1.5% of the generated Cl_2 reacted with the Ce foil. In future experiments, a hydriding step will be added to increase the surface area of the sample to be chlorinated.

Figure 12. Ce foil before (left) and (after) chlorination.

After the experiment, a yellow-orange solid (see Figure 13) had accumulated on the exterior of the quartz crucible in a ring, just at the end of the heating zone in the tube furnace.

This is an Accepted Manuscript of an article published by Taylor & Francis in *Nuclear Technology* on February 28th 2024, available at: https://doi.org/10.1080/00295450.2023.2299908

This solid is thought to be $NiCl_2$, because: (1) its color is characteristic of anhydrous $NiCl_2$; (2) it turned green when exposed to atmosphere, which is characteristic of the anhydrous to hydrate reaction; (3) when analyzed with ICP-MS, Ni was detected; and (4) the Cl^- ion-selective electrode confirmed the solid to be 91.5 ± 10% chloride. This $NiCl_2$ was likely a corrosion product from the chlorination of the Ni reactor.

Figure 13. Salt block after REE chlorination experiment. Full block (left) and bisected (right).

The quartz crucible also had cracks at the base alongside the melted salt block which fractured when the crucible was set down. These cracks may have been due to an aggressive cooling rate (10 °C/min) and/or mechanical stresses induced during cooling by deposited metals (e.g., Ca, La) in contact with the quartz crucible (see Figure 13). Future experiments will use alumina crucibles to avoid cracking.

4. Conclusion

A small-scale apparatus for simultaneous Cl_2 electrosynthesis and REE chlorination was demonstrated and evaluated using electrochemical, mass spectroscopic, and gravimetric

This is an Accepted Manuscript of an article published by Taylor & Francis in *Nuclear Technology* on February 28th 2024, available at: https://doi.org/10.1080/00295450.2023.2299908

methods. Pt and graphite proved to be appropriate anode materials, and graphite anodes were used to generate Cl_2 via electrolysis. A QMS analyzed the output of the reactor, showed the successful generation of Cl_2 by electrolysis, and indicated that CO and CO_2 were also produced at the anode. CO and CO_2 were likely produced because of O^{2-} that was produced via hydrolysis during drying. To demonstrate the apparatus' ability to chlorinate REE, a piece of Ce foil was suspended over the electrochemical cell and was chlorinated by Cl_2 produced at the anode. Future work will focus on scaling up the system to kilogram scale quantities, decreasing the required chlorination time, and investigating the apparatus' ability to chlorinate samples more fully and volatilize away impurities from the sample being chlorinated.

Acknowledgements

This work was funded by the U.S. Department of Energy by Lawrence Livermore National Laboratory (LLNL) under contract DE-AC52-07NA27344. We would like to thank Jake Monson for his assistance with the project.

Declaration of Interest Statement

The authors declare that they have no known competing financial interests or personal relationships that could have appeared to influence the work reported in this paper.

References

[1] U.S.G. Survey, Mineral commodity summaries 2022, U.S. Geological Survey, 2022. https://doi.org/10.3133/mcs2022.
[2] M. Kurata, K. Kinoshita, T. Hijikata, T. Inoue, Conversion of Simulated High-level Liquid Waste to Chloride for the Pretreatment of Pyrometallurgical Partitioning Process, J. Nucl. Sci. Technol. 37 (2000) 682–690. https://doi.org/10.1080/18811248.2000.9714944.
[3] G. Charalampides, K.I. Vatalis, B. Apostoplos, B. Ploutarch-Nikolas, Rare Earth Elements: Industrial Applications and Economic Dependency of Europe, Procedia Econ. Finance. 24 (2015) 126–135. https://doi.org/10.1016/S2212-5671(15)00630-9.

[4] Rare Earth Elements—Critical Resources for High Technology | USGS Fact Sheet 087-02, (n.d.). https://pubs.usgs.gov/fs/2002/fs087-02/ (accessed August 30, 2023).
[5] P. Okabe, D. Rappleye, M. Newton, M.F. Simpson, Development of metallic nuclear material purification process via simultaneous chlorination and volatilization, J. Nucl. Mater. 543 (2021) 152626. https://doi.org/10.1016/j.jnucmat.2020.152626.
[6] S. Boyd, C. Taylor, 3 - Chemical fundamentals and applications of molten salts, in: T.J. Dolan (Ed.), Molten Salt React. Thorium Energy, Woodhead Publishing, 2017: pp. 29–91. https://doi.org/10.1016/B978-0-08-101126-3.00003-8.
[7] M.F. Simpson, Projected Salt Waste Production from a Commercial Pyroprocessing Facility, Sci. Technol. Nucl. Install. 2013 (2013) e945858. https://doi.org/10.1155/2013/945858.
[8] D. Yoon, S. Paek, J.-H. Jang, J. Shim, S.-J. Lee, Actinide Drawdown From LiCl-KCl Eutectic Salt via Galvanic/chemical Reactions Using Rare Earth Metals, 방사성폐기물학회지. 18 (2020) 373–382.
[9] T. Inoue, M. Sakata, H. Miyashiro, T. Matsumura, A. Sasahara, N. Yoshiki, Development of Partitioning and Transmutation Technology for Long-Lived Nuclides, Nucl. Technol. 93 (1991) 206–220. https://doi.org/10.13182/NT91-A34506.
[10] J.H. Goode, A Laboratory Study of the Separation and Recovery of Uranium and Plutonium from Fission Products by Chloride Volatility, Oak Ridge National Lab., Oak Ridge, TN, 1964.
[11] D. Bradley, The preparation and properties of the chlorides of uranium, plutonium, and thorium and of the fission product chlorides, Great Britain Atomic Energy Research Establishment, Harwell (United Kingdom), 1957. https://www.osti.gov/biblio/4321371 (accessed February 15, 2023).
[12] J.L. Moriarty, Vapor Pressures of Yttrium and Rare Earth Chlorides Above Their Melting Points., J. Chem. Eng. Data. 8 (1963) 422–424. https://doi.org/10.1021/je60018a041.
[13] Z. Singh, R. Prasad, V. Venugopal, D.D. Sood, The vaporization thermodynamics of uranium tetrachloride, J. Chem. Thermodyn. 10 (1978) 129–134. https://doi.org/10.1016/0021-9614(78)90118-0.
[14] The Vapor Pressure of Plutonium Halides | The Journal of Chemical Physics | AIP Publishing, (n.d.). https://pubs.aip.org/aip/jcp/article/18/5/713/72617/The-Vapor-Pressure-of-Plutonium-Halides (accessed August 30, 2023).
[15] Vapor Pressure and Enthalpies of Vaporization of Cerium Trichloride, Tribromide, and Triiodide | Journal of Chemical & Engineering Data, (n.d.). https://pubs.acs.org/doi/full/10.1021/je000035e (accessed August 30, 2023).
[16] Vapor Pressures of the Rare-Earth Metals | The Journal of Chemical Physics | AIP Publishing, (n.d.). https://pubs.aip.org/aip/jcp/article/41/9/2818/209433/Vapor-Pressures-of-the-Rare-Earth-Metals (accessed August 30, 2023).
[17] D.R. Stull, Vapor Pressure of Pure Substances. Organic and Inorganic Compounds, Ind. Eng. Chem. 39 (1947) 517–540. https://doi.org/10.1021/ie50448a022.
[18] M. Schvaneveldt, R. Fuller, D. Rappleye, Electroanalytical measurements of lanthanum (III) chloride in molten calcium chloride and molten calcium chloride and lithium chloride, J. Electroanal. Chem. 918 (2022) 116442. https://doi.org/10.1016/j.jelechem.2022.116442.
[19] M. Schvaneveldt, In-Situ Chlorine Gas Generation for Chlorination and Purification of Rare Earth and Actinide Metals, Brigham Young University, 2022. https://scholarsarchive.byu.edu/etd/9707 (accessed April 11, 2023).

This is an Accepted Manuscript of an article published by Taylor & Francis in *Nuclear Technology* on February 28th 2024, available at: https://doi.org/10.1080/00295450.2023.2299908

[20] H. Yin, L. Gao, H. Zhu, X. Mao, F. Gan, D. Wang, On the development of metallic inert anode for molten CaCl2–CaO System, Electrochimica Acta. 56 (2011) 3296–3302. https://doi.org/10.1016/j.electacta.2011.01.026.
[21] Corrosion: Environments and Industries, 2006. https://doi.org/10.31399/asm.hb.v13c.9781627081849.
[22] Pamphlet 164) Reactivity and Compatibility of Chlorine and Sodium Hydroxide with Various Materials, Bookstore.ChlorineInstitute.Org. (n.d.). http://bookstore.chlorineinstitute.org/pamphlet-164-reactivity-and-compatibility-of-chlorine-and-sodium-hydroxide-with-various-materials-158.html?Session_ID=4534bf2a57fa9c931400e4a7a0362e31 (accessed June 15, 2023).
[23] W. Zhang, C.R. Pulham, A.R. Mount, N. Brockie, R. Lewin, Thermodynamic calculation and reference electrode calibration for high temperature molten salts, Energy Mater. 3 (2008) 132–136. https://doi.org/10.1179/174892408X394254.
[24] I. Barin, Thermochemical Data of Pure Substances, 3rd ed., VCH Verlagsgesellschaft mbH., Weinheim, 1995.
[25] M.W. Chase, JANAF Thermochemical Tables, NIST Standard Reference Database 13, (1986). https://doi.org/10.18434/T42S31.
[26] Chemical Name Search, (n.d.). https://webbook.nist.gov/chemistry/name-ser/ (accessed June 12, 2023).
[27] Electrochemical Investigation of Moisture Byproducts in Molten Calcium Chloride by Rankin Shum, Marah Fuller, Tyler Williams, Devin Rappleye :: SSRN, (n.d.). https://papers.ssrn.com/sol3/papers.cfm?abstract_id=4459979 (accessed August 28, 2023).
[28] S. Natsui, R. Shibuya, R.O. Suzuki, T. Kikuchi, A. Ito, T. Sato, R. Yamamoto, H. Nogami, Quantification of the Impact of Residual H2O on Cathodic Behavior in Molten CaCl2 Electrolysis, J. Sustain. Metall. 8 (2022) 532–540. https://doi.org/10.1007/s40831-022-00516-w.
[29] C. Zhang, D. Rappleye, A. Nelson, S. Simpson, M. Simpson, Electroanalytical Measurements of Oxide Ions in Molten CaCl2 on W electrode, J. Electrochem. Soc. 168 (2021) 097502. https://doi.org/10.1149/1945-7111/ac208e.
[30] A. Mukherjee, R. Kumaresan, S. Ghosh, Redox behaviour of CaCl2 melts in presence of moisture as impurity. Part I: Cyclic voltammetry, J. Electroanal. Chem. 902 (2021) 115778. https://doi.org/10.1016/j.jelechem.2021.115778.
[31] M. Molenda, J. Stengler, M. Linder, A. Wörner, Reversible hydration behavior of CaCl2 at high H2O partial pressures for thermochemical energy storage, Thermochim. Acta. 560 (2013) 76–81. https://doi.org/10.1016/j.tca.2013.03.020.
[32] H.U. Rammelberg, T. Schmidt, W. Ruck, Hydration and dehydration of salt hydrates and hydroxides for thermal energy storage - kinetics and energy release, Energy Procedia. 30 (2012) 362–369. https://doi.org/10.1016/j.egypro.2012.11.043.
[33] H. Kondo, Z. Asaki, Y. Kondo, Hydrolysis of fused calcium chloride at high temperature, Metall. Trans. B. 9 (1978) 477–483. https://doi.org/10.1007/BF02654424.
[34] M. Mohamedi, B. Børresen, G.M. Haarberg, R. Tunold, Anodic Behavior of Carbon Electrodes in CaO - CaCl2 Melts at 1123 K, J. Electrochem. Soc. 146 (1999) 1472. https://doi.org/10.1149/1.1391789.
[35] H. Xie, H. Zhao, Q. Song, Z. Ning, J. Qu, H. Yin, Anodic Gases Generated on a Carbon Electrode in Oxide-Ion Containing Molten CaCl2 for the Electro-Deoxidation Process, J. Electrochem. Soc. 165 (2018) E759. https://doi.org/10.1149/2.0251814jes.

This is an Accepted Manuscript of an article published by Taylor & Francis in *Nuclear Technology* on February 28th 2024, available at: https://doi.org/10.1080/00295450.2023.2299908

Table 1. Estimations of E^0 from thermochemical data.

Redox Couple	E^0 **(V vs. Cl^-/Cl_2, 1 atm)**	E^0 **(V vs. Ag/AgCl, 5 mol%)**
Ag/Ag^+	-0.814	0.278
Ni/Ni^{2+}	-0.754	0.338
W/W^{2+}	-0.699	0.393
Mo/Mo^{4+}	-0.641	0.451
W/W^{6+}	-0.277	0.815
Mo/Mo^{6+}	-0.140	0.952
Pt/Pt^{2+}	-0.111*	0.981
Cl^-/Cl_2	0.000	1.092
C/C^{4+}	0.215	1.307
*Extrapolated from available thermodynamic data		

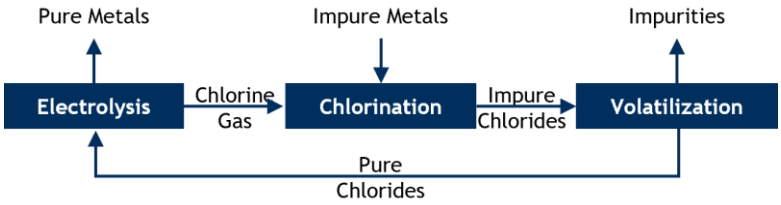

Figure 1. Proposed chloride volatility process.

This is an Accepted Manuscript of an article published by Taylor & Francis in *Nuclear Technology* on February 28th 2024, available at: https://doi.org/10.1080/00295450.2023.2299908

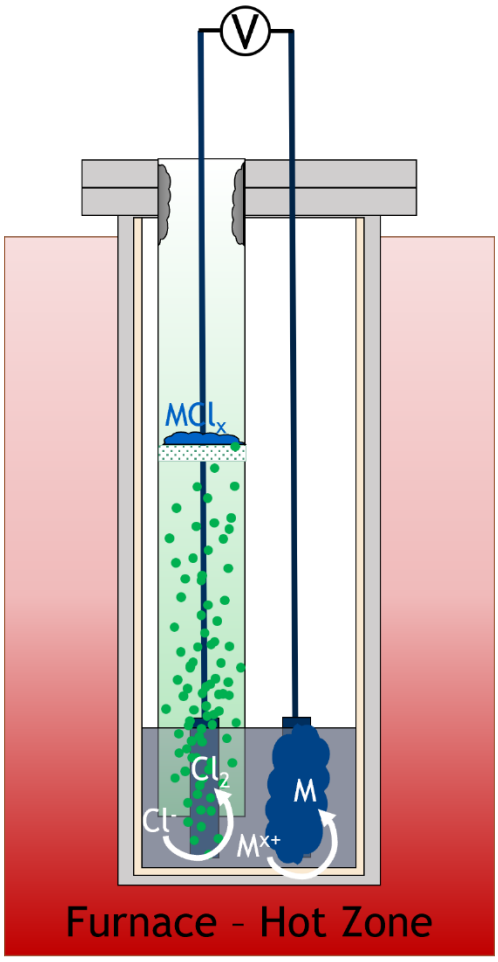

Figure 2. Generic schematic for the proposed chloride volatility process.

This is an Accepted Manuscript of an article published by Taylor & Francis in *Nuclear Technology* on February 28th 2024, available at: https://doi.org/10.1080/00295450.2023.2299908

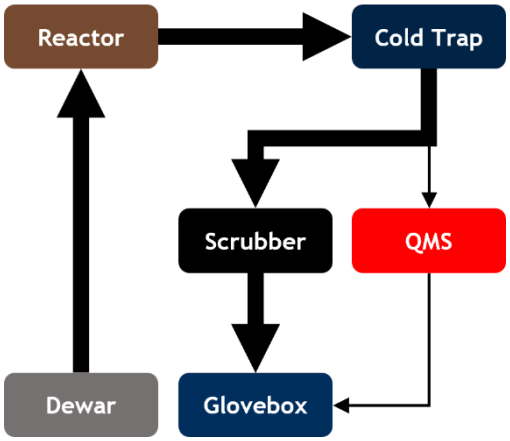

Figure 3. Simplified PFD for gas lines associated with Cl_2 synthesis and analysis. Line thickness indicates relative volumetric flow rates.

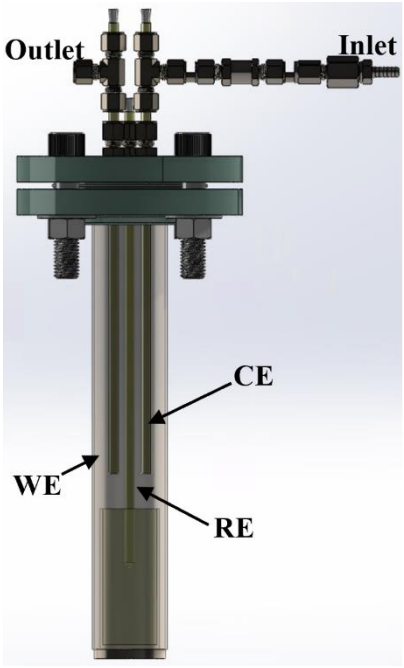

Figure 4. Schematic of reactor featuring interior. Electrodes are missing, but their alumina feedthroughs are present.

This is an Accepted Manuscript of an article published by Taylor & Francis in *Nuclear Technology* on February 28th 2024, available at: https://doi.org/10.1080/00295450.2023.2299908

Figure 5. Quartz Crucible and Basket. Side-by-side (left) and nested (right) views.

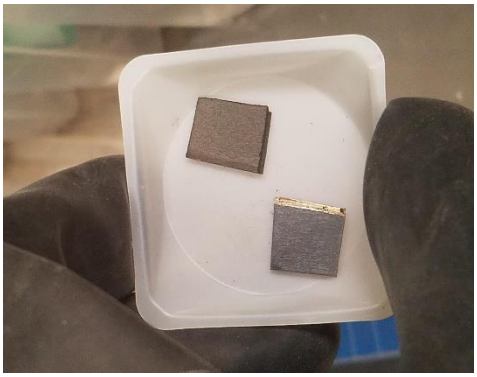

Figure 6. Cerium foil before chlorination. Dark, grey oxide layer removed before chlorination with 220 grit sandpaper.

This is an Accepted Manuscript of an article published by Taylor & Francis in *Nuclear Technology* on February 28th 2024, available at: https://doi.org/10.1080/00295450.2023.2299908

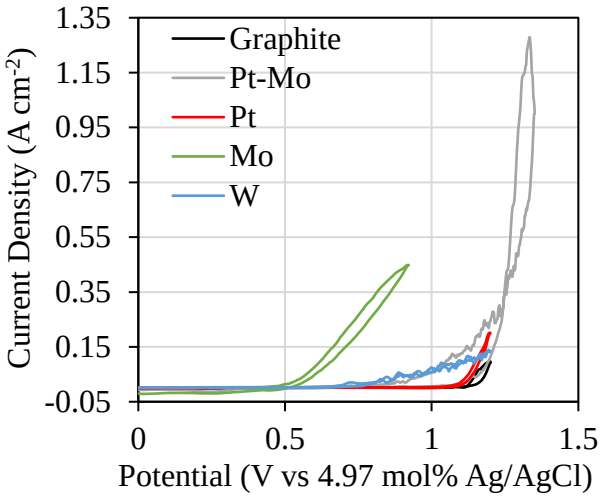

Figure 7. Current density versus potential for 2 wt% $LaCl_3$ in $CaCl_2$ at 825°C and 10 mV s^{-1}, *iR* compensated. 3.174 mm W rod CE.

This is an Accepted Manuscript of an article published by Taylor & Francis in *Nuclear Technology* on February 28th 2024, available at: https://doi.org/10.1080/00295450.2023.2299908

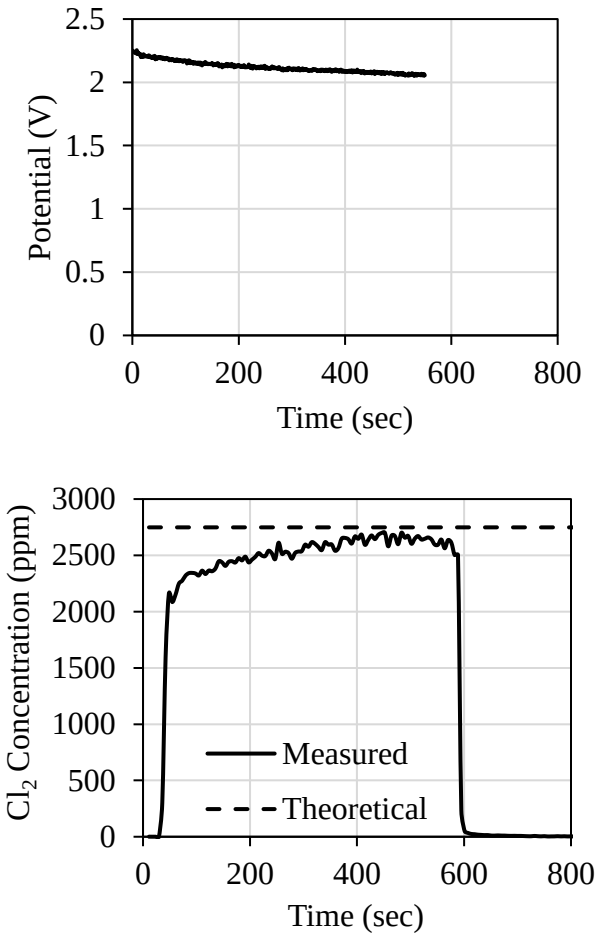

Figure 8. Electrochemical (top) and QMS (bottom) response to a current of 1.5 A applied to a Mo/Pt/La/La^{3+},Ca^{2+},Cl^{-}/Cl_2/$C_{graphite}$ cell (WE geometric area: 2.3 cm^2). Approximately 4 LPM N_2 flowed through the reactor as carrier gas.

This is an Accepted Manuscript of an article published by Taylor & Francis in *Nuclear Technology* on February 28th 2024, available at: https://doi.org/10.1080/00295450.2023.2299908

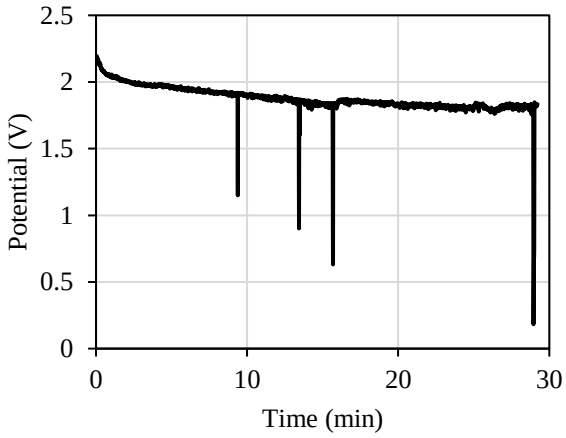

Figure 9. Electrochemical response to a current of 1.5 A applied to a $Mo/Pt/La/La^{3+},Ca^{2+},Cl^{-}/Cl_2/C_{graphite}$ cell (WE geometric area: 2.3 cm^2). Approximately 0.1 LPM of Ar flowed through the reactor as carrier gas.

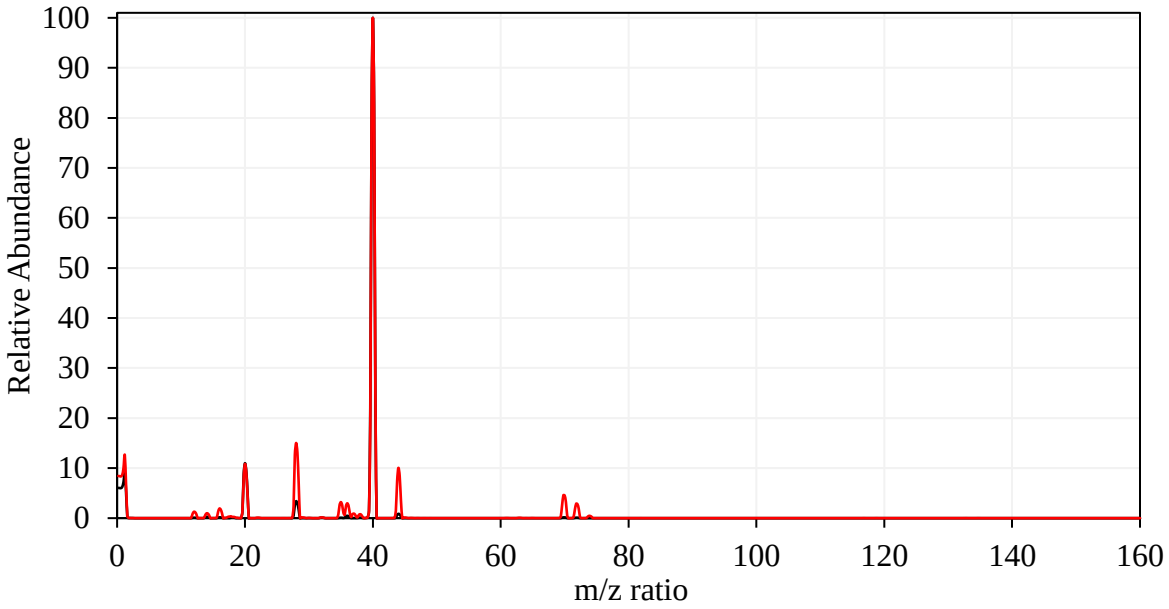

Figure 10. Mass spectra from 30 minutes (black) and 40 minutes (red) into 1.5 A (2.3 cm^2) electrolysis with 0.1 LPM Ar of carrier gas.

This is an Accepted Manuscript of an article published by Taylor & Francis in *Nuclear Technology* on February 28th 2024, available at: https://doi.org/10.1080/00295450.2023.2299908

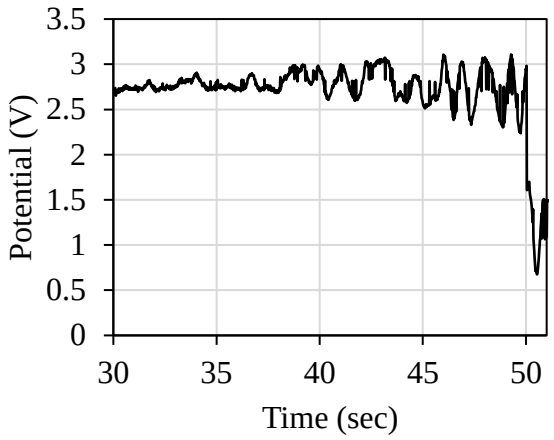

Figure 11. Electrochemical response of 1.5 A applied to a Mo/Pt/La/La^{3+},Ca^{2+},Cl^-/Cl_2/$C_{graphite}$ cell (WE geometric area: 1.77 cm^2). No Ar was pushed through the reactor during electrolysis.

Figure 12. Ce foil before (left) and (after) chlorination.

This is an Accepted Manuscript of an article published by Taylor & Francis in *Nuclear Technology* on February 28th 2024, available at: https://doi.org/10.1080/00295450.2023.2299908

Figure 13. Salt block after REE chlorination experiment. Full block (left) and bisected (right).

This is an Accepted Manuscript of an article published by Taylor & Francis in *Nuclear Technology* on February 28th 2024, available at: https://doi.org/10.1080/00295450.2023.2299908